A new method for sensitivity analysis of photonic crystal devices

Georgios Veronis, Robert W. Dutton, and Shanhui Fan

Department of Electrical Engineering, Stanford University, Stanford, California 94305

ABSTRACT

We present a new method for sensitivity analysis of photonic crystal devices and nanophotonic devices in general. The algorithm is based on the finite-difference frequency-domain method and uses the adjoint variable method and perturbation theory techniques. We show that our method is highly efficient and accurate and can be applied to the calculation of the sensitivity of transmission parameters of resonant nanophotonic devices.

Keywords: Sensitivity analysis, photonic crystal devices, fabrication disorders

1. INTRODUCTION

For practical implementations of photonic crystal devices, it is of fundamental importance to determine the sensitivity of the device properties to fabrication-related disorders.[1–5] In principle, the sensitivity can be determined by varying the device parameters in the vicinity of the design point, and by calculating the response functions of the resulting perturbed devices. However, such a direct approach is computationally inefficient, since it requires a full analysis for each variation of the design parameters. Moreover, in practice it is important to determine the sensitivity with respect to variations of geometrical parameters. In the commonly-used finite-difference time-domain (FDTD) method, a variation of the device size by a single grid point may already lead to large structural change. Consequently, in order to determine the sensitivity accurately in the direct approach, a high-resolution grid is typically needed, further increasing the computational cost.

In this paper, we introduce a new approach for sensitivity analysis of photonic crystal structures based upon the adjoint variable method[6] (AVM) and perturbation theory in a frequency-domain solver for Maxwell's equations. In this approach, once a simulation for the device properties is performed, the sensitivity with respect to any number of design parameters is calculated with very small additional computational cost. Furthermore, this approach determines the sensitivity with respect to geometrical parameter variations accurately without the need for the use of high-resolution grids. We expect this approach to be important for fast computational prototyping of practical photonic crystal and nanophotonic devices.

2. FORMULATION

2.1. Finite-difference frequency-domain method

In frequency-domain, the wave equation for the electric field is

$$[-\nabla \times \nabla \times + k_0^2 \epsilon_r]\mathbf{E} = \nabla \times \mathbf{M} + j\omega\mu_0\mathbf{J} \tag{1}$$

where $k_0^2 = \omega^2\epsilon_0\mu_0$ and $\mathbf{J}$ ($\mathbf{M}$) is the electric (magnetic) source current. To solve this equation, we use a finite-difference frequency-domain (FDFD) method.[7] The fields are discretized on a nonuniform orthogonal grid truncated by a perfectly matched layer (PML) in its coordinate stretching formulation.[8] The spatial discretization of Eq. (1) on the grid results in a system of complex linear equations. The equation for the field at each grid point involves only the fields at the six (four in 2-D) adjacent grid points. Thus the resulting system matrix is sparse.

2.2. Adjoint variable method

The system of linear equations resulting from discretizing Eq. (1) is of the general form

$$\mathbf{Z}(\mathbf{s})\mathbf{I} = \mathbf{V} \tag{2}$$

where $\mathbf{Z}$ is the system matrix, $\mathbf{s}$ is the vector of design parameters, $\mathbf{I}$ is the vector of unknown fields, and $\mathbf{V}$ is the source which does not depend on $\mathbf{s}$ ($\nabla_s \mathbf{V} = 0$), since we focus on variations of the device structure. The response function of interest is a function of the field $T = T(\mathbf{I}(\mathbf{s}))$ and therefore has no explicit dependence on $\mathbf{s}$. The objective of the sensitivity analysis is to determine the gradient of the response function with respect to the design parameters $\nabla_s T$. Using AVM, it can be shown that[6]

$$\nabla_s T = -\hat{\mathbf{I}}^T (\nabla_s \mathbf{Z})\mathbf{I} \tag{3}$$

$$\mathbf{Z}^T \hat{\mathbf{I}} = [\nabla_{\mathbf{I}} T]^T \tag{4}$$

where $\mathbf{I}$, obtained from Eq. (2), is the vector of fields at the current design point, and $\hat{\mathbf{I}}$ is the solution to the so-called *adjoint problem* (Eq. (4)). In our case, the matrix $\mathbf{Z}$ obtained from Eq. (1) is symmetric. Thus, Eq. (4) requires determining the field when the source is the *adjoint excitation* $\hat{\mathbf{V}} = [\nabla_{\mathbf{I}} T]^T$, which is the gradient of the response with respect to the fields. As an example, if the response function is defined as the field intensity at a given monitor point, the adjoint excitation will be nonzero only at the monitor point.

In summary, sensitivity analysis using the adjoint variable method consists of three steps. First, the electromagnetic fields $\mathbf{I}$ at a specific design point are calculated by solving Eq. (2). Second, the adjoint problem is solved (Eq. (4)). In the adjoint problem the device structure is unperturbed but the source is the adjoint excitation, which is nonzero only at the monitor points. Once the field $\mathbf{I}$ and the adjoint field $\hat{\mathbf{I}}$ are calculated, the sensisitivity is obtained by the summation in Eq. (3). In the case of sensitivity analysis with respect to fabrication disorders, this summation has to be carefully considered, as discussed below. If we are interested in the sensitivity with respect to many different design parameters we only need to solve Eqs. (2) and (4) once. For each design parameter the sensitivity is then obtained through Eq. (3).

2.3. Sparse matrix solution method

A particularly efficient approach to solve Eqs. (2) and (4) is the use of a direct sparse matrix method, which requires only a single LU decomposition of $\mathbf{Z}$ and two back-substitutions. Having calculated $\mathbf{I}$ and $\hat{\mathbf{I}}$, the sensitivity with respect to *any* number of design parameters is obtained by calculating $\nabla_s \mathbf{Z}$ which has a negligible computational cost. Thus, when a direct solver is used, the only additional cost required for the sensitivity analysis is one back-substitution for the solution of Eq. (4), which is typically at least an order of magnitude smaller than the cost of the LU decomposition.

2.4. Sensitivity to material parameter variations

In the device sensitivity analysis, we are interested in the effects of variations of the dielectric function $\epsilon_r = \epsilon_r(\mathbf{r})$ on the response function of the device. To calculate the effect of varying the dielectric constant ϵ_{r1} of a particular device (assuming that the entire device region has the same dielectric constant ϵ_{r1}), it is straightforward to calculate $\nabla_s \mathbf{Z}$, and then, using Eq. (3), one obtains

$$\frac{\partial T}{\partial \epsilon_{r1}} = -k_0^2 \sum_i \hat{I}_i I_i \tag{5}$$

where the summation is taken over the volume of this device.

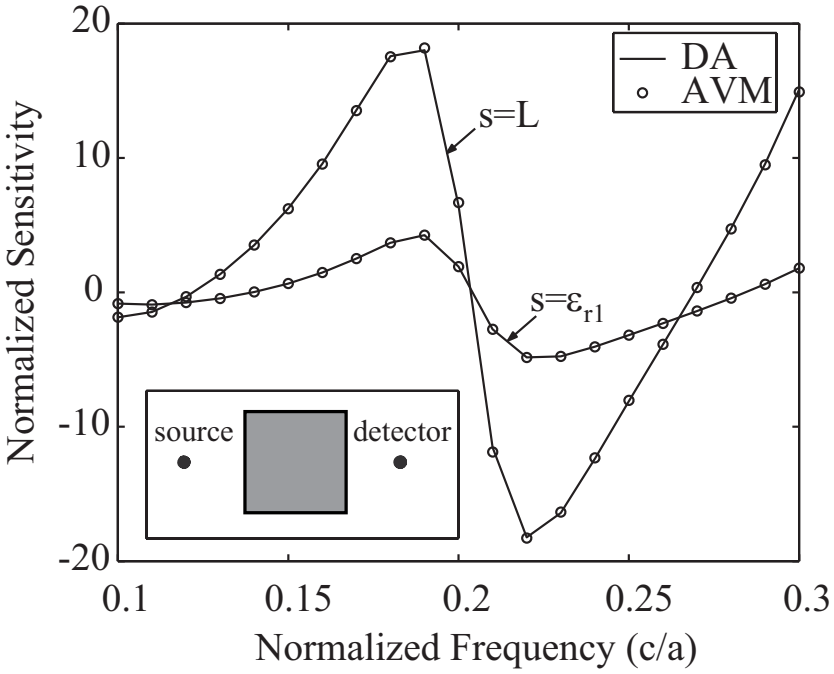

Figure 1. Comparison of the DA and AVM methods in high-resolution grids (160 points per a). We show the normalized sensitivity of the transmission defined as $\frac{\partial T}{\partial s}(\frac{T}{s})^{-1}$ (s is either the square size L or ϵ_{r1}) as a function of frequency. The structure, a dielectric block, is shown in the inset and L =0.9375a, ϵ_{r1} =11.56.

2.5. Sensitivity to fabrication disorders

In practice, it is particularly useful to determine the tolerance of the device performance to fabrication disorders. In this case, we are interested in the effect of perturbations due to shifting of the interface between regions with different dielectric constants. Suppose we have two regions with dielectric constants ϵ_{r1} and ϵ_{r2}. Since $\epsilon_r(\mathbf{r})$ is a step function, its derivative is a delta function, so that the summation in Eq. (3) is limited to the interface between the two media. This surface summation needs to be carefully defined, due to the discontinuity of the normal component of the electric field $E_\perp$ to the interface, and has recently been studied by Johnson *et al.*[9] in the context of perturbation theory. Following their approach, we showed that

$$\frac{\partial T}{\partial s} = -k_0^2 \sum_i \Delta l_i^{-1} \frac{dh(\mathbf{r}_{\mathrm{surf}i}, s)}{ds} [\Delta\epsilon_{12} \hat{E}_{\|i} E_{\|i} - \Delta(\epsilon_{12}^{-1}) \hat{D}_{\perp i} D_{\perp i}] \tag{6}$$

where $\Delta\epsilon_{12} \equiv \epsilon_{r1} - \epsilon_{r2}$, $\Delta(\epsilon_{12}^{-1}) \equiv \epsilon_0^{-2}(\epsilon_{r1}^{-1} - \epsilon_{r2}^{-1})$, Δl_i is the local grid size normal to the interface, and the summation is taken over the interface. The function $h = h(\mathbf{r}_{\mathrm{surf}}, s)$ defined on the boundary surface is the distance that the interface between regions 1 and 2 shifts towards region 2. The summation in Eq. (6) is well-defined, since both $E_\|$ and $D_\perp$ are continuous at the interface.

2.6. Two-dimensional formulation

We focus on 2-D calculations as a proof of principle. For TE polarization we have $\mathbf{E} = E_z\hat{z}$ and the wave equation for the electric field becomes[8]

$$[\frac{\partial^2}{\partial x^2} + \frac{\partial^2}{\partial y^2} + k_0^2\epsilon_r]E_z = j\omega\mu_0 J_z \tag{7}$$

Similarly, for TM polarization we have $\mathbf{H} = H_z\hat{z}$ and

$$[\frac{\partial}{\partial x}(\frac{1}{\epsilon_r}\frac{\partial}{\partial x}) + \frac{\partial}{\partial y}(\frac{1}{\epsilon_r}\frac{\partial}{\partial y}) + k_0^2]H_z = j\omega\epsilon_0 M_z \tag{8}$$

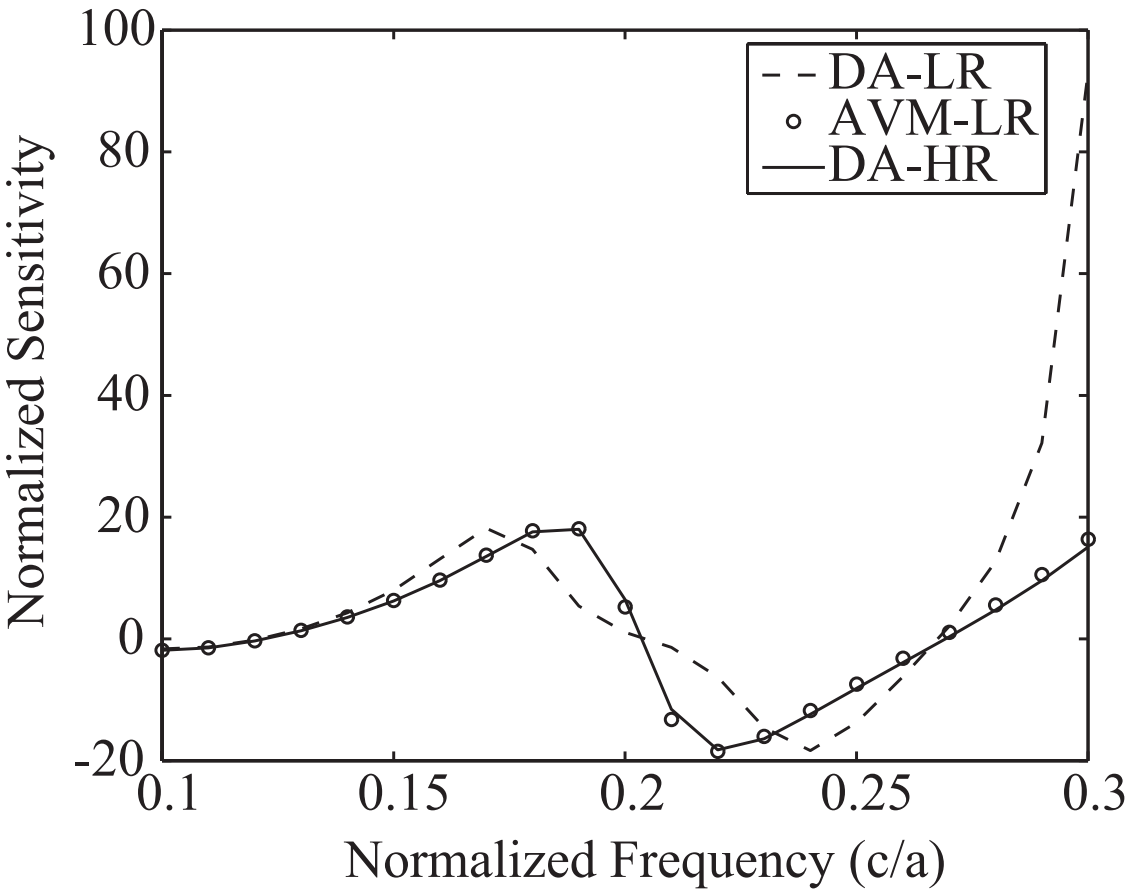

Figure 2. Comparison of the DA and AVM methods in low-resolution grids (16 points per a) with the benchmark DA in high-resolution grid (160 points per a) for $s = L$.

In the TM case, $\mathbf{I}$ and $\hat{\mathbf{I}}$ correspond to magnetic fields. To use Eq. (6) where the sensitivity is calculated in terms of the electric field, we first solve Eq. (8) to determine H_z, from which $E_{\|}$ and $D_{\perp}$ can then be calculated. The adjoint problem can also be recast in terms of the magnetic field. If the response function is defined as $T = |H_{\text{obs}}|^2$ where H_{obs} is the field at the observation point, we can show that the adjoint source is $\hat{M}_z = -\frac{2}{j\omega\mu_0} H^*_{\text{obs}}$ at the observation point and zero elsewhere.

3. METHOD VALIDATION

To validate our method, we compare it with the direct approach (DA),[6] in which sensitivity is simply calculated as

$$\frac{\partial T}{\partial s} \simeq \frac{T(s + \Delta s/2) - T(s - \Delta s/2)}{\Delta s} \tag{9}$$

We choose a high-resolution grid (160 points per a, where a is a length used for normalization). In Fig. 1 we show the sensitivity of the response function, calculated with the DA and our method for the structure shown in the inset of Fig. 1. We observe that there is excellent agreement over the entire frequency range.

4. ACCURACY AND EFFICIENCY OF THE METHOD

Since our method uses a perturbative approach for the calculation of sensitivity, we expect it to be accurate even when a low-resolution grid is used. To verify this, we compare our method in a low-resolution grid (16 points

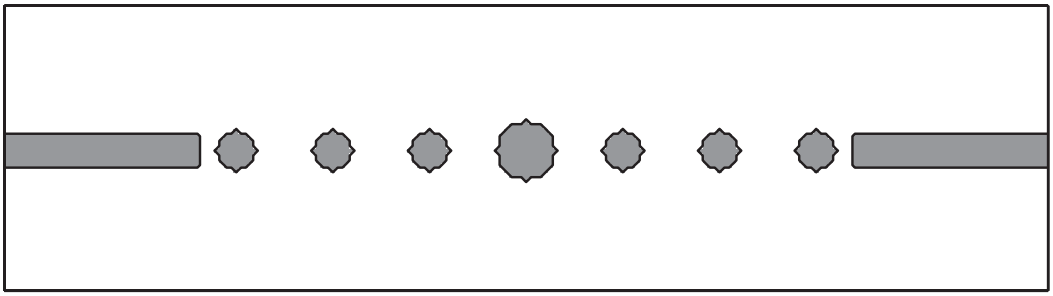

Figure 3. Device geometry of a photonic-crystal band-pass filter.

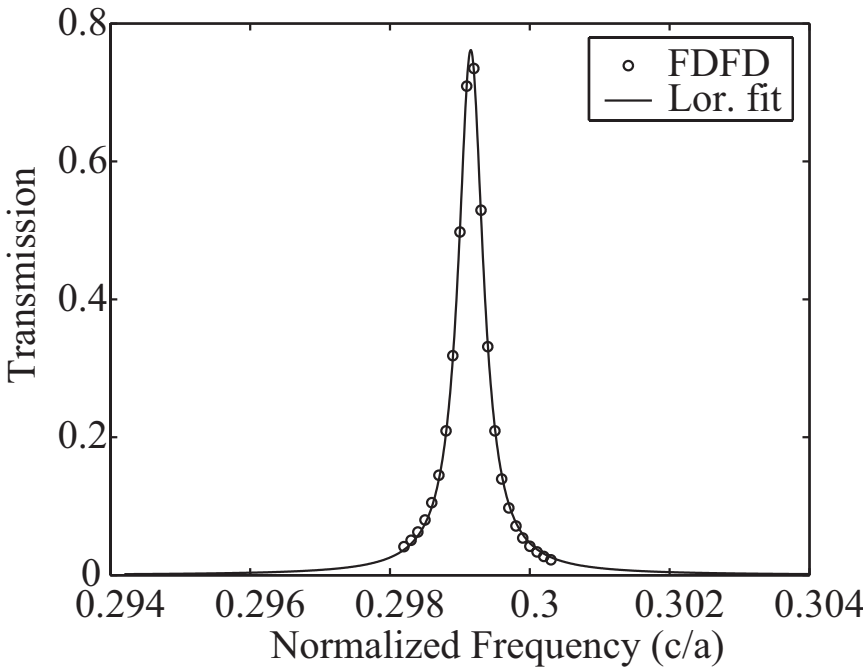

Figure 4. Transmission spectrum calculated by FDFD and the corresponding Lorentzian fit for a photonic-crystal-based band-pass optical filter (the device geometry is shown in Fig. 3). The distance between adjacent rods is a and their radius is $0.2a$. The radius of the central dielectric rod is r_d=$0.4a$. The width of the dielectric waveguides is $0.35a$, and their distance from the center of the closest rod is $0.4a$.

per a) to the benchmark DA in the high-resolution grid (160 points per a). Results are shown in Fig. 2 for the sensitivity with respect to the object size. The agreement is very good over the entire frequency range in spite of the 10 times coarser grid. In Fig. 2 we also show the result obtained by the DA in the low-resolution grid. We observe that the DA, when applied to a low-resolution grid, introduces very large error especially at high frequencies.

Our method is significantly more efficient than the DA. The DA requires two full solutions at design points $s+\Delta s/2$ and $s-\Delta s/2$ (including both the LU decomposition and the back-substitution) for *each* design parameter. Thus, for n design parameters a total of $2n+1$ full analyses are required. Our method, as mentioned above, requires only one additional back-substitution, irrespective of the number of design parameters.

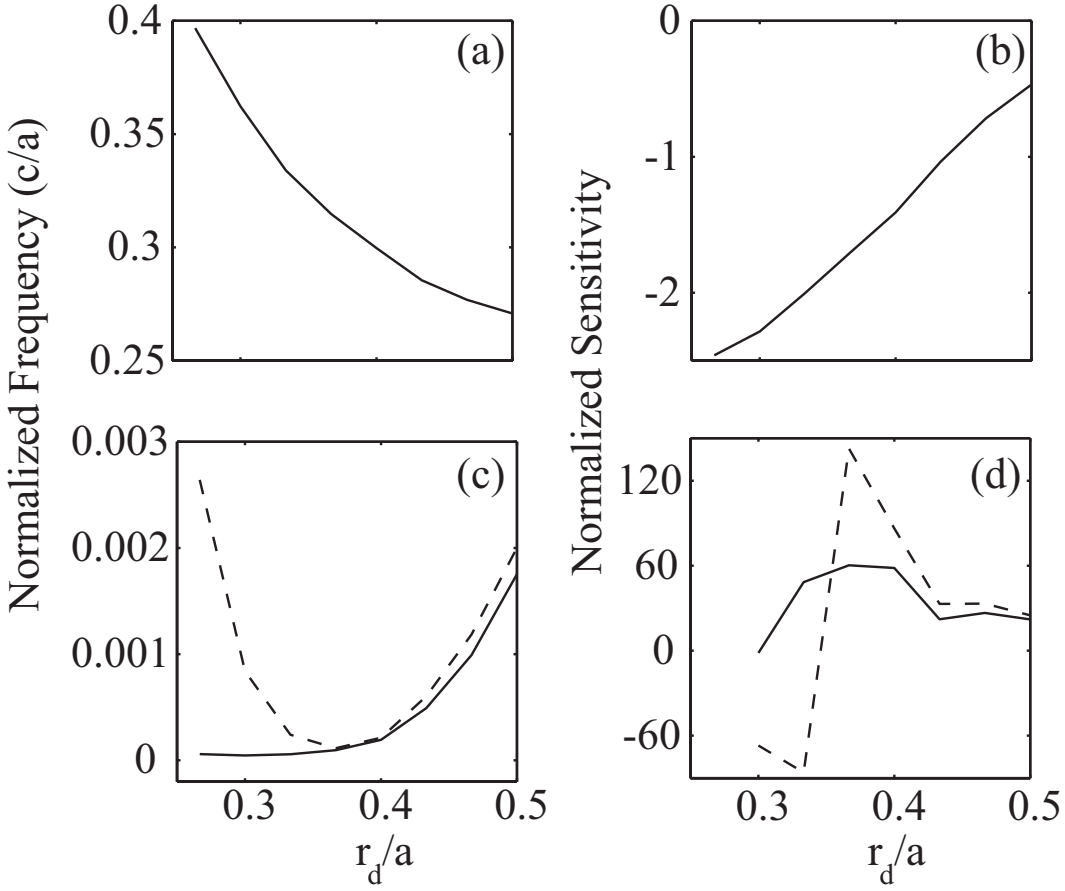

Figure 5. (a) Ω_0, (c) Ω_1, Ω_2 (shown with a dashed line) as a function of the radius of the central dielectric rod r_d. Normalized sensitivities (b) $\frac{\partial\Omega_0}{\partial r_d}(\frac{\Omega_0}{a})^{-1}$, (d) $\frac{\partial\Omega_1}{\partial r_d}(\frac{\Omega_1}{a})^{-1}$, $\frac{\partial\Omega_2}{\partial r_d}(\frac{\Omega_2}{a})^{-1}$ (shown with a dashed line) as a function of r_d.

5. SENSITIVITY OF TRANSMISSION PARAMETERS OF RESONANT NANOPHOTONIC DEVICES

As an application of our method, we calculate the sensitivity of the resonant frequency and the bandwidth of an optical filter. One photonic-crystal band-pass filter geometry[10] is shown in Fig. 3. The transmission spectrum of such a device close to the resonant frequency can be very well approximated by a Lorentzian shape

$$T(\omega) = \frac{\Omega_1^2}{(\omega - \Omega_0)^2 + {\Omega_2}^2} \tag{10}$$

as shown in Fig. 4, where Ω_0 is the resonant frequency, and Ω_1, Ω_2 are bandwidths.

To calculate $\frac{\partial \Omega_0}{\partial s}$, $\frac{\partial \Omega_1}{\partial s}$, $\frac{\partial \Omega_2}{\partial s}$. we differentiate Eq. (10) to obtain

$$\frac{\partial T(\omega_i)}{\partial s} = \frac{\partial T(\omega_i)}{\partial \Omega_0}\frac{\partial \Omega_0}{\partial s} + \frac{\partial T(\omega_i)}{\partial \Omega_1}\frac{\partial \Omega_1}{\partial s} + \frac{\partial T(\omega_i)}{\partial \Omega_2}\frac{\partial \Omega_2}{\partial s} \tag{11}$$

Here, $\frac{\partial T(\omega_i)}{\partial s}$ is calculated using the method described above. In addition, $\frac{\partial T(\omega_i)}{\partial \Omega_0}$, $\frac{\partial T(\omega_i)}{\partial \Omega_1}$, $\frac{\partial T(\omega_i)}{\partial \Omega_2}$ can be analytically calculated from Eq. (10), once the transmission spectrum is fitted with a Lorentzian. Thus, one can determine $\frac{\partial \Omega_0}{\partial s}$, $\frac{\partial \Omega_1}{\partial s}$, $\frac{\partial \Omega_2}{\partial s}$ if Eq. (11) is applied to a minimum of three frequency points close to Ω_0. In practice, more accurate results are obtained if more than three frequency points are used, and the overdetermined system is solved in the least-squares sense. Alternatively, $\frac{\partial \Omega_0}{\partial s}$, $\frac{\partial \Omega_1}{\partial s}$, $\frac{\partial \Omega_2}{\partial s}$ can be obtained if we differentiate some other function of the transmission spectrum such as T^{-1}

$$-T(\omega_i)^{-2}\frac{\partial T(\omega_i)}{\partial s} = \frac{\partial T(\omega_i)^{-1}}{\partial \Omega_0}\frac{\partial \Omega_0}{\partial s} + \frac{\partial T(\omega_i)^{-1}}{\partial \Omega_1}\frac{\partial \Omega_1}{\partial s} + \frac{\partial T(\omega_i)^{-1}}{\partial \Omega_2}\frac{\partial \Omega_2}{\partial s} \tag{12}$$

Depending on the design point, either Eq. (11) or Eq. (12) results in a better least-squares fit. In each case, we use the one which provides the best fit to our results.

In Figs. 5a, 5c we show the calculated Ω_0, Ω_1, Ω_2 for the device structure of Fig. 3, as a function of the radius of the central dielectric rod r_d. We observe that Ω_0 decreases as r_d increases, and that both Ω_1 and Ω_2 are much smaller than Ω_0 due to the high-Q defect dipole-mode formed by modifying r_d.[10] In Figs. 5b, 5d we show the calculated sensitivities of Ω_0, Ω_1, Ω_2. We observe that Ω_1, Ω_2 are much more sensitive to variations in r_d than Ω_0. The calculated Ω_0, Ω_1, Ω_2 are consistent with previously published results,[10] and their calculated sensitivities are consistent with the values obtained by the DA in the same grid.

ACKNOWLEDGMENTS

This research was supported by DARPA/MARCO under the Interconnect Focus Center.

REFERENCES

1. K.-C. Kwan, X. Zhang, Z.-Q. Zhang, and C. T. Chan, "Effects due to disorder on photonic crystal-based waveguides," *Appl. Phys. Lett.* **82**, pp. 4414–4416, 2003.
2. A. Chutinan and S. Noda, "Effects of structural fluctuations on the photonic bandgap during fabrication of a photonic crystal," *J. Opt. Soc. Am. B* **16**, pp. 240–244, 1999.
3. Z.-Y. Li and Z.-Q. Zhang, "Fragility of photonic band gaps in inverse-opal photonic crystals," *Phys. Rev. B* **62**, pp. 1516–1519, 2000.
4. A. A. Asatryan, P. A. Robinson, L. C. Botten, R. C. McPhedran, N. A. Nicorovici, and C. M. de Sterke, "Effects of geometric and refractive index disorder on wave propagation in two-dimensional photonic crystals," *Phys. Rev. E* **62**, pp. 5711–5720, 2000.
5. S. Fan, P. R. Villeneuve, and J. D. Joannopoulos, "Theoretical investigation of fabrication-related disorder on the properties of photonic crystals," *J. Appl. Phys.* **78**, pp. 1415–1418, 1995.
6. N. K. Georgieva, S. Glavic, M. H. Bakr, and J. W. Bandler, "Feasible adjoint sensitivity technique for EM design optimization," *IEEE Trans. Microwave Theory Tech.* **50**, pp. 2751–2758, 2002.

7. S. D. Wu and E. N. Glytsis, "Finite-number-of-periods holographic gratings with finite-width incident beams: analysis using the finite-difference frequency-domain method," *J. Opt. Soc. Am. A* **19**, pp. 2018–2029, 2002.
8. J. Jin, *The Finite Element Method in Electromagnetics*, John Wiley & Sons, New York, 2002.
9. S. G. Johnson, M. Ibanescu, M. A. Skorobogatiy, O. Weisberg, J. D. Joannopoulos, and Y. Fink, "Perturbation theory for Maxwell's equations with shifting material boundaries," *Phys. Rev. E* **65**, pp. 066611/1–7, 2002.
10. S. G. Johnson, S. Fan, A. Mekis, and J. D. Joannopoulos, "Multipole-cancellation mechanism for high-Q cavities in the absence of a complete photonic band gap," *Appl. Phys. Lett.* **78**, pp. 3388–3390, 2001.